J|A|C|S
ARTICLES
Published on Web 02/18/2006

NMR Studies of Solvent-Assisted Proton Transfer in a Biologically Relevant Schiff Base: Toward a Distinction of Geometric and Equilibrium H-Bond Isotope Effects

Shasad Sharif,[†] Gleb S. Denisov,[‡] Michael D. Toney,[§] and Hans-Heinrich Limbach*,[†]

Contribution from the Institut für Chemie, Takustrasse 3, Freie Universität Berlin, D-14195 Berlin, Germany, the Institute of Physics, St. Petersburg State University, 198504 St. Petersburg, Russian Federation, and the Department of Chemistry, University of California-Davis, Davis, California 95616

Received September 11, 2005; E-mail: limbach@chemie.fu-berlin.de

Abstract: The tautomeric equilibrium in a Schiff base, *N*-(3,5-dibromosalicylidene)-methylamine **1**, a model for the hydrogen bonded structure of the cofactor pyridoxal-5′-phosphate PLP which is located in the active site of the enzyme, was measured by means of ^{1}H and ^{15}N NMR and deuterium isotope effects on ^{15}N chemical shifts at variable temperature and in different organic solvents. The position of the equilibrium was estimated using the one-bond ^{1}J(OHN) and vicinal ^{3}J(H_{α}CNH) scalar coupling constants. Additionally, DFT calculations of a series of Schiff bases, *N*-(R_1-salicylidene)-alkyl(R_2)amines, were performed to obtain the hydrogen bond geometries. The latter made it possible to investigate a broad range of equilibrium positions. The increase of the polarity of the aprotic solvent shifts the proton in the intramolecular OHN hydrogen bond closer to the nitrogen. The addition of methanol and of hexafluoro-2-propanol to **1** in aprotic solvents models the PLP−water interaction in the enzymatic active site. The alcohols, which vary in acidity and change the polarity around the hydrogen bond, also stabilize the equilibrium, so that the proton is shifted to the nitrogen.

Introduction

In various enzymatic transformations of amino acids, e.g., racemization, decarboxylation, and transamination, the cofactor pyridoxal-5′-phosphate PLP[1,2] plays an important role.[3−5] According to the crystal structures of PLP-dependent enzymes,[6−10] the cofactor is embedded in a hydrogen bonded network and forms a Schiff base as either an "internal aldimine" or an "external aldimine" with the ϵ-amino group of a lysine residue or with the amino acid substrates which are going to be transformed. Of special importance are two functional OHN-hydrogen bonds as illustrated in Scheme 1.[1] In the first step of the catalytic cycle (not shown), it is assumed that the bridging proton of the intramolecular OHN-hydrogen bond has to be transferred from the hydroxyl oxygen to the imino nitrogen, a process which is assisted by protonation of the pyridine ring.[1]

Scheme 1. PLP "Internal Aldimine" in Asparate Amino Transferase

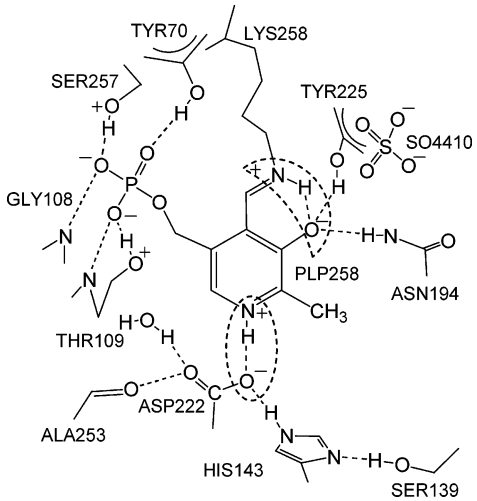

The role of the intermolecular OHN hydrogen bond is not clear: it could first serve as an attachment point of the cofactor with the protein, as the phosphate group, but it could also assist the proton transfer in the intramolecular OHN hydrogen bond.

To model the intermolecular OHN-hydrogen bond, in a series of papers some of us have studied various acid-pyridine or collidine (2,4,6-trimethylpyridine) complexes using liquid- and solid-state NMR techniques.[11−17] Information about the hydrogen bond geometries, H/D isotope effects on the latter, and zero-

[†] Freie Universität Berlin.
[‡] St. Petersburg State University.
[§] University of California-Davis.

(1) Christen, P.; Metzler, D. E. *Transaminases*; Wiley: New York, 1985.
(2) Fujiwara, T. *Bull. Chem. Soc. Jpn.* **1973**, *46*, 863−871.
(3) Spies, M. A.; Toney, M. D. *Biochemistry* **2003**, *42*, 5099−5107.
(4) Malashkevich, V. N.; Toney, M. D.; Jansonius, J. N. *Biochemistry* **1993**, *32*, 13451−13462.
(5) Zhou, X.; Toney, M. D. *Biochemistry* **1999**, *38*, 311−320.
(6) Jager, J.; Moser, M.; Sauder, U.; Jansonius, J. N. *J. Mol. Biol.* **1994**, *239*, 285−305.
(7) Smith, D. L.; Almo, S. C.; Toney, M. D.; Ringe, D. *Biochemistry* **1989**, *28*, 8161−8167.
(8) Shaw, J. P.; Petsko, G. A.; Ringe, D. *Biochemistry* **1997**, *36*, 1329−1342.
(9) Stamper, C. G. F.; Morollo, A. A.; Ringe, D. *Biochemistry* **1998**, *37*, 10438−10445.
(10) Jansonius, J. N. *Curr. Opin. Struct. Biol.* **1998**, *8*, 759−769.

Scheme 2. Schematic View of the Keto−Enol Tautomerism of *N*-(3,5-Dibromosalicylidene)-methylamine **1** and the Influence of Alcohols[a]

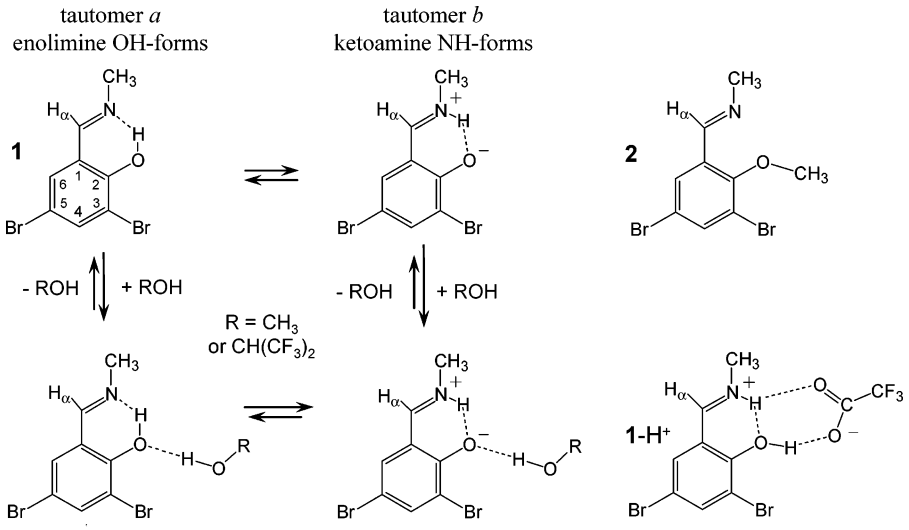

[a] Also shown are the adduct **1**−H$^+$ with trifluoroacetic acid and *N*-(2-methoxybenzylidene)-methylamine **2**. Only the zwitterionic resonance structure is shown for tautomer b for which one could also discuss a quinoid neutral structure.

point energy changes were obtained as a function of the position of the proton in the bridge. Moreover, solvent effects on the hydrogen bond geometries were studied.[18] In principle, the data could be explained in terms of single-well potentials for the proton motion in the nonsymmetric cases and in terms of low-barrier hydrogen bonds when the average proton position was localized in the hydrogen bond center.

To study the properties of the intramolecular OHN-hydrogen bond model Schiff bases have been studied where the intermolecular OHN-bridge was removed. For example, a Schiff base has been studied[19,20] where the pyridine nitrogen was methylated. As this compound is poorly soluble in aprotic organic solvents, the pyridine ring has also been replaced by other aryl groups leading to substituted *N*-(salicylidene)-methylamines. As an example, the derivative *N*-(3,5-dibromosalicylidene)-methylamine **1** is depicted in Scheme 2a. Using UV−vis[21] spectrosopy and ^{13}C,[22] ^{17}O,[23,24] and ^{15}N[25] NMR spectroscopy, it has been shown that these compounds exhibit a keto−enol tautomerism between an OH- (enol) and an NH- (keto) form.[26−29] Many factors, such as the local polarity or the presence of water, influence the equilibrium. Especially the analysis of coupling constants ^1J(O<u>H</u>N) and ^{15}N chemical shifts δ(OH<u>N</u>) provides information about the equilibrium constants of the tautomerism. In addition, H/D isotope effects on NMR chemical shifts have been observed providing information about equilibrium isotope effects.

A problem of the previous studies has been the interpretation of the H/D isotope effects on the NMR parameters. These effects can arise both (i) from equilibrium isotope effects which imply a different equilibrium constant of the tautomerism for H as compared to D and (ii) from intrinsic isotope effects on the spectral parameters. The intrinsic effects are caused by isotope effects on the hydrogen bond geometries, which themselves originate in anharmonic ground-state vibrations. The latter can also have a small influence on the equilibrium isotope effects because their zero-point energies are different than in the case of harmonic vibrations.

The scope of this paper is, therefore, to make a first step toward a distinction of both types of isotope effects. For this purpose, we have performed a liquid-state NMR study of **1** as a function of temperature, solvent, dielectric constant, and addition of methanol and hexafluoro-2-propanol (HFIP) in order to mimic the intermolecular hydrogen bonds of the intramolecular OHN-bridge to the enzyme. For comparison, we also studied the protonated form of **1** and *N*-(2-methoxybenzylidene)-methylamine **2** (Scheme 2) where the intramolecular OHN hydrogen bond is suppressed by replacement of the OH group by a methoxy group.

Due to this variation, a very large range of the tautomerism, from a dominant enol- to a dominant keto-form, could be

(11) Benedict, H.; Limbach, H. H.; Wehlan, M.; Fehlhammer, W. P.; Golubev, N. S.; Janoschek, R. *J. Am. Chem. Soc.* **1998**, *120*, 2939−2950.
(12) Lorente, P.; Shenderovich, I. G.; Golubev, N. S.; Denisov, G. S.; Buntkowsky, G.; Limbach, H. H. *Magn. Reson. Chem.* **2001**, *39*, S18−S29.
(13) Foces-Foces, C.; Llamas-Saiz, A. L.; Lorente, P.; Golubev, N. S.; Limbach, H. H. *Acta Crystallogr.* **1999**, *C55*, 377−381.
(14) Smirnov, S. N.; Benedict, H.; Golubev, N. S.; Denisov, G. S.; Kreevoy, M. M.; Schowen, R. L.; Limbach, H. H. *Can. J. Chem.* **1999**, *77*, 943−949.
(15) Shenderovich, I. G.; Tolstoy, P. M.; Golubev, N. S.; Smirnov, S. N.; Denisov, G. S.; Limbach, H. H. *J. Am. Chem. Soc.* **2003**, *125*, 11710−11720.
(16) Limbach, H. H.; Pietrzak, M.; Benedict, H.; Tolstoy, P. M.; Golubev, N. S.; Denisov, G. S. *J. Mol. Struct.* **2004**, *706*, 115−119.
(17) Limbach, H. H.; Pietrzak, M.; Sharif, S.; Tolstoy, P. M.; Shenderovich, I. G.; Smirnov, S. N.; Golubev, N. S.; Denisov, G. S. *Chem.—Eur. J.* **2004**, *10*, 5195−5204.
(18) Tolstoy, P. M.; Smirnov, S. N.; Shenderovich, I. G.; Golubev, N. S.; Denisov, G. S.; Limbach, H. H. *J. Mol. Struct.* **2004**, *700*, 19−27.
(19) Heyl, D.; Luz, E.; Harris, S. A.; Folkers, K. *J. Am. Chem. Soc.* **1951**, *73*, 3430−3433.
(20) Kondo, H.; Kikuchi, J.; Uchida, S.; Kitamikado, T.; Koyanagi, E.; Sunamoto, J. *Bull. Chem. Soc. Jpn.* **1985**, *58*, 675−681.
(21) Rospenk, M.; Krol-Starzomska, I.; Filarowski, A.; Koll, A. *Chem. Phys.* **2003**, *287*, 113−124.
(22) Rozwadowski, Z.; Dziembowska, T. *Magn. Reson. Chem.* **1999**, *37*, 274−278.
(23) Zhuo, J. C. *Magn. Reson. Chem.* **1999**, *37*, 259−268.
(24) Kozerski, L.; Kawecki, R.; Krajewski, P.; Kwiecien, B.; Boykin, D. W.; Bolvig, S.; Hansen, P. E. *Magn. Reson. Chem.* **1998**, *36*, 921−928.
(25) Dziembowska, T.; Rozwadowski, Z.; Filarowski, A.; Hansen, P. E. *Magn. Reson. Chem.* **2001**, *39*, 67−80.
(26) Hansen, P. E.; Sitkowski, J.; Stefaniak, L.; Rozwadowski, Z.; Dziembowska, T. *Ber. Bunsen-Ges. Phys. Chem.* **1998**, *102*, 410−413.
(27) Rozwadowski, Z.; Majewski, E.; Dziembowska, T.; Hansen, P. E. *J. Chem. Soc., Perkin Trans. 2* **1999**, 2809−2817.
(28) Schilf, W.; Kamienski, B.; Dziembowska, T.; Rozwadowski, Z.; Szady-Chelmieniecka, A. *J. Mol. Struct.* **2000**, *552*, 33−37.
(29) Kamienski, B.; Schilf, W.; Dziembowska, T.; Rozwadowski, Z.; Szady-Chelmieniecka, A. *Solid State NMR* **2000**, *16*, 285−289.

explored. By expanding a data analysis developed previously,[11−17] for intermolecular OHN-bridges we show that both the geometries and zero-point energies of the OH- as well as of the NH-forms depend on temperature and the environment, i.e., to substantial variations of the tautomeric equilibria.

This paper is organized as follows. After an Experimental and a Theoretical Section where the formalism of the data analysis is described, the results are reported and discussed.

Materials and Methods

Materials. 3,5-Dibromosalicylaldehyde, 2-methoxybenzaldehyde, methanol, and hexafluoro-2-propanol (1,1,1,3,3,3-hexafluoro-2-propanol, HFIP) were purchased from Aldrich. ^{15}N-Labeled *N*-(3,5-dibromosalicylidene)-methylamine **1** was synthesized by condensing 3,5-dibromosalicylaldehyde with 95% ^{15}N-enriched methylamine hydrochloride (Chemotrade) in methanolic solution by adding an equivalent amount of sodium hydroxide, according to the method described by Hansen et al.[26−28] The product was characterized by mass spectrometry and ^{1}H liquid-state NMR. The ^{15}N-isotopic enrichment of 90−95% was determined by mass spectroscopy. *N*-(2-Methoxybenzylidene)-methylamine **2** was synthesized from 2-methoxybenzaldehyde by treating it with an aqueous solution of methylamine, according to the method described by Cromwell et al.[30,31] The product was characterized by ^{1}H liquid-state NMR spectroscopy. Deuterated solvents: toluene-d_8, methanol-d_1/-d_3/-d_4, chloroform-d_1, dichloromethane-d_2, and trifluoroacetic acid-d_1 were purchased from Deutero GmbH. The deuterated Freon gas mixture CDF_3/$CDClF_2$ was synthesized from chloroform-d_1.[32,33] The mole fraction of CDF_3 0.4 in the Freon mixture was defined by integration of the residual proton NMR signals at 140 K.

NMR Measurements. The liquid-state ^{1}H and ^{15}N NMR spectra were measured using a Bruker AMX 500 spectrometer (500.13 MHz for ^{1}H, 50.68 MHz for ^{15}N) equipped for low-temperature NMR down to 100 K. The solvents used were toluene-d_8, methanol-d_3/-d_4, chloroform-d_1, dichloromethane-d_2, trifuoroacetic acid-d_1, and a liquefied deuterated Freon gas mixture CDF_3/$CDClF_2$ whose properties have been described previously.[33] The ^{1}H spectra were referenced to TMS by using toluene-d_8 (2.03 ppm), methanol-d_3/d_4 (3.31 ppm), chloroform-d_1 (7.27 ppm), and dichloromethane-d_2 (5.31 ppm) signals as internal references. In the case of the Freon mixture the central component of the $CHClF_2$ triplet was set to 7.18 ppm.[33] The recycle times were between 3 and 5 s. Standard ^{15}N NMR inverse proton decoupled spectra were recorded with a recycle time of 3 s. Especially, in the case of **1**−H$^+$ the non-^{1}H-decoupled ^{15}N spectrum was recorded with 400 scans.

To reference the ^{15}N chemical shifts of **1** observed for the different deuterated solvents using a ^{2}H field locking to external neat nitromethane we proceeded as follows. We prepared neat samples of nitromethane containing capillaries with the various deuterated solvents and measured the ^{15}N spectra under the same field locking conditions as the samples of **1**. As the preparation of a capillary using deuterated Freon was difficult, the ^{15}N referencing of the Freon samples was done without field locking. To convert the ^{15}N chemical shifts of the nitromethane scale into the solid $^{15}NH_4Cl$ scale, the relation $\delta(CH_3NO_2, \text{liq.}) = \delta(^{15}NH_4Cl, \text{solid}) - 341.168$ ppm[34] was used.

NMR Samples. A. Solution of 1 in Trifluoroacetic Acid. The Schiff base **1** decomposes in acid media. All attempts to measure its spectra in aqueous hydrochloric acid HCl, in fluoroboric acid HBF_4, or in picric acid solution in dichloromethane failed. Only in trifluoroacetic acid ($pK_a = 0.2$[35]) **1**−H$^+$ is stable for a short time. The nondecoupled ^{15}N NMR spectra were recorded immediately after dissolving **1** in trifluoroacetic acid with a lock on a capillary with trifluoroacetic acid-d_1.

B. Solutions of 1 in Other Aprotic Organic Solvents. ^{1}H spectra of a 2 mM solution of **1** in chloroform-d_1 were measured in the temperature range 205−260 K. ^{1}H and ^{15}N spectra of solution of **1** in toluene-d_8 were measured in the temperature range 180−240 K; concentrations of **1** were 2 mM for ^{1}H NMR and 15 mM for ^{15}N NMR spectra. ^{1}H and ^{15}N spectra of a solution of **1** in dichloromethane-d_2 were measured in the temperature range 190−270 K. Concentrations of **1** were 2 mM for ^{1}H NMR and 30 mM and 45 mM for nondeuterated and deuterated **1** for ^{15}N NMR spectra. **1** was deuterated by repeated dissolution in methanol-d_1 and evaporation of the solvent in high vacuum overnight. The deuteration fraction achieved was 0.66 as estimated by ^{1}H NMR. ^{1}H and ^{15}N spectra of a 3 mM solution of **1** in a deuterated Freon mixture were measured in the temperature range 114 to 190 K. **1** is not soluble in the Freon mixture at low temperature, but when it is fast cooled to 140 K it stays in a glassy condition long enough to measure ^{15}N NMR spectra.

C. Addition of Alcohols. Defined quantities of methanol, AH = CH_3OH or CH_3OD ($pK_a = 15.5$[35]), were added to a 45 mM solution of deuterated **1** in dichloromethane-d_2 and to a 3 mM solution of **1** in the Freon mixture. Adding methanol to a solution of **1** in the Freon mixture required preparation of the series of samples with different values of *R*. The deuteration ratio x_D was changed by adding a mixture of methanol/methanol-d_1. The molar alcohol/substrate ratios $R = C_{AH}/C$, where *C* represents the total concentration of **1**, were estimated by integration of the signal of nonexchangeable protons of the alcohol with respect to the aromatic proton signals H4 of **1**. The measurements in methanol-d_3 or methanol-d_4 at 190 K were done at a concentration of 7 mM. Fluorinated alcohol HFIP AH = $(CF_3)_2CHOH$ ($pK_a = 9.30$[36]) was added to a 30 mM solution of **1** in dichloromethane-d_2. Only ratios of $R = 2.5$ could be achieved because of the precipitation of HFIP in dichloromethane at 190 K.

DFT Calculations. All quantum chemical calculations of geometry, energy, and vibrational frequencies were carried out with the GAUSSIAN98 program[37] on an Origin 2000 (SGI) computer with 16 processors MIPS R10000 and three Gigabyte memory.

The ab initio method used is the density functional theory (DFT) with the B3LYP[38,39] functional, combined with standard basis set 6-31++G(d) for geometry optimizations for modeling of the hydrogen bonding. After each geometry optimization, a calculation of the vibrational frequencies was performed in order to ensure that the calculated geometry corresponds to a (local) minimum and not to a saddle point on the energy hypersurface.

For chemical shielding calculations, the gauge independent atomic orbital (GIAO)[40] method approach was used in combination with the DFT method and the basis set 6-311++G(d,p).[41] It is generally accepted that this use of an improved basis set increases the accuracy of the calculated chemical shielding.[42] The principal components of the calculated chemical shielding tensors are absolute shielding values; i.e., $\sigma = 0$ corresponds to the shielding of the "bare" nucleus. The chemical shielding values σ were converted to chemical shifts using the relation $\delta = A - \sigma$,[43,42] where $A = 257.868$ ppm is the absolute chemical shielding

(30) Cromwell, N. H.; Hoeksema, H. *J. Am. Chem. Soc.* **1945**, *67*, 1658−1660.
(31) Cromwell, N. H.; Babson, R. D.; Harris, C. E. *J. Am. Chem. Soc.* **1943**, *65*, 312−315.
(32) Siegel, J. S.; Anet, F. A. L. *J. Org. Chem.* **1988**, *53*, 2629−2630.
(33) Shenderovich, I. G.; Burtsev, A. P.; Denisov, G. S.; Golubev, N. S.; Limbach, H. H. *Magn. Reson. Chem.* **2001**, *39*, S91−S99.
(34) Hayashi, S.; Hayamizu, K. *Bull. Chem. Soc. Jpn.* **1991**, *64*, 688−690.
(35) Bartberger, M. D.; Fukuto, J. M.; Houk, K. N. *Proc. Nat. Acad. Sci.* **2001**, *98*, 2194−2198.
(36) Middleton, W. J.; Lindsey, R. V., Jr. *J. Am. Chem. Soc.* **1964**, *86*, 4948−4952.
(37) Frisch, M. J.; Pople, J. A. *Gaussian98*, 98 ed.; Gaussian, Inc.: Pittsburgh, PA, 1998.
(38) Becke, A. D. *J. Chem. Phys.* **1993**, *98*, 5648−5652.
(39) Lee, C.; Yang, W.; Parr, R. G. *Phys. Rev.* **1988**, *B37*, 785−789.
(40) Wolinski, K.; Hinton, J. F.; Pulay, P. *J. Am. Chem. Soc.* **1990**, *112*, 8251−8260.
(41) Buhl, M.; Kaupp, M.; Malkina, O. L.; Malkin, V. G. *J. Comput. Chem.* **1999**, *20*, 91−105.
(42) Dokalik, A.; Kalchhauser, H.; Mikenda, W.; Schweng, G. *Magn. Reson. Chem.* **1999**, *37*, 895−902.

Scheme 3. Variables Characterizing the Geometry of a Hydrogen Bond

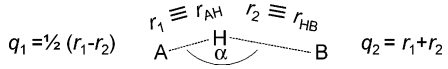

of gaseous ammonia used as a primary reference. To convert these data into the solid $^{15}NH_4Cl$ scale, the relation $\delta(CH_3NO_2, \text{liq.}) = \delta(NH_3, \text{gas}) + 398.9$ ppm[43] was used.

Theoretical Section

Geometric Hydrogen Bond Correlations. In a number of papers it has been shown[45−50] the valence bond orders or bond valences defined by Pauling[51] are useful for describing geometric correlations of hydrogen bonds of the general type A−H···B. In addition, they are useful in order to derive correlations of NMR parameters with hydrogen bond geometries.[11−17]

The bond valences of the A−H and of the H···B bonds are defined as

$$p_1 = \exp\{-(r_1 - r_1^\circ)/b_1\} \text{ and } p_2 = \exp\{-(r_2 - r_2^\circ)/b_2\} \quad (1)$$

Here, $r_1 = r_{AH}$ represents the A...H distance, $r_2 = r_{HB}$, the H...B distance, and p_1 and p_2, the corresponding valence bond orders of the diatomic units as illustrated in Scheme 3. r_1° and r_2° represent the equilibrium distances in the fictive free diatomic units AH and HB, and b_1 and b_2, the parameters describing the decays of the bond order when the bond is stretched. According to Brown[52] the total valence of hydrogen is unity, i.e.

$$p_1 + p_2 = 1 \quad (2)$$

Therefore, it follows that r_1 and r_2 depend on each other. It is, however, more convenient to express the correlation in terms of the hydrogen bond coordinates $q_1 = {}^1/_2(r_1 - r_2)$ and $q_2 = r_1 + r_2$. For a linear hydrogen bond, q_1 represents the distance of H from the hydrogen bond center, and q_2, the distance between the heavy atoms A and B, as indicated in Scheme 3.

Note that the correlation does not depend on the hydrogen bond angle α. In this paper, A corresponds to oxygen, and B, to the nitrogen atom of **1** in the intramolecular OHN hydrogen bond, shown in Scheme 2.

The parameters of eqs 1 and 2 for OHO-, OHN-, and NHN-hydrogen bonds were obtained by fitting low-temperature neutron diffraction data available in the Cambridge Structural Database (CSD).[45] A typical correlation curve of q_2 vs q_1 will be presented later (dashed line in Figure 4a); it shows that when the proton is transferred from A to B, a hydrogen bond contraction occurs which is maximum when the proton is located approximately in the hydrogen bond center.

Recently, some of us noticed, however, that in the case of very strong NHN-[16] and OHN-[17] hydrogen bonds the observed heavy atom distances q_2 were larger in the symmetric configuration than the predicted minimum value. In addition, it was not possible to describe H/D isotope effects on the hydrogen bond geometries in terms of eqs 1 and 2. Therefore, it was assumed that these equations are valid only for equilibrium geometries, as zero-point vibrations were not taken into account. To take the latter into account, we proposed the following empirical equations for the calculation of isotope sensitive bond orders from the equilibrium bond orders[17]

$$p_1^{\,L} = p_1 - c^L(p_1p_2)^f(p_1 - p_2) - d^L(p_1p_2)^g = \exp\{-(r_1^{\,L} - r_1^\circ)/b_1\}$$

$$p_2^{\,L} = p_2 + c^L(p_1p_2)^f(p_1 - p_2) - d^L(p_1p_2)^g = \exp\{-(r_2^{\,L} - r_2^\circ)/b_2\},\ L = H, D \quad (3)$$

The parameters c^L and d^L, L = H, D and the values of the powers f and g have been adapted empirically to the case of OHN-hydrogen bonds to pyridine.[17] To some extent, these parameters depend on whether the data points which are included correspond to hydrogen bonds without or with a small barrier for the proton motion.[17] A typical corrected q_2 vs q_1 curve will be presented later (dotted line in Figure 4a). In summary, eq 3 allows one to calculate the *primary* as well as the *secondary* geometric hydrogen bond isotope effect, i.e.

$$\Delta q_1 \equiv q_1^{\,D} - q_1^{\,H} \text{ and } \Delta q_2 \equiv q_2^{\,D} - q_2^{\,H} \quad (4)$$

Δq_1 represents roughly the different location of D as compared to H with respect to the hydrogen bond center, and Δq_2, the change of the heavy atom locations after deuteration.

Isotope Fractionation in Hydrogen Bonded Systems. The zero-point energy correction of eq 3 influences substantially the correlation analysis of isotopic H/D fractionation between the OHN-hydrogen-bonded complexes and reference complexes XHY, characterized by the equation

$$AHB + XDY \rightleftharpoons ADB + XHY \quad (5)$$

The equilibrium constant of this reaction is given by

$$K = \frac{1}{\phi} = \frac{x_{ADB}x_{XHY}}{x_{AHB}x_{XDY}} \approx \exp\left(-\frac{\Delta ZPE}{RT}\right) \quad (6)$$

The inverse value K represents the fractionation factor ϕ, x_i are mole fractions or concentrations of the various isotopic species, R is the gas constant, T is the temperature, and ΔZPE is the zero-point energy (ZPE) difference of the H and D forms of the reacting hydrogen bonded complexes

$$\Delta ZPE = ZPE(XHY) - ZPE(XDY) - [ZPE(AHB) - ZPE(ADB)] \quad (7)$$

In principle, it would be desirable to express the values of ZPE(ALB), L = H, D, as a function of the corrected bond valences $p_1^{\,L}$ and $p_2^{\,L}$ from which ΔZPE could be calculated as a function of the hydrogen bond geometries. Unfortunately, general correlations for all isotopic sensitive vibrations and, therefore, of their ZPE values are not available at present. Therefore, we use the following approximation, in which ΔZPE is expressed as a function of the equilibrium bond valences p_1 and p_2 as has been proposed previously,[14,17]

(43) Macholl, S.; Boerner, F.; Buntkowsky, G. *Z. Phys. Chem.* **2003**, *217*, 1473−1505.
(44) Jameson, C. J.; Jameson, A. K.; Oppusunggu, D.; Wille, S.; Burrell, P. M.; Mason, J. *J. Chem. Phys.* **1981**, *74*, 81−88.
(45) Steiner, T.; Saenger, W. *Acta Crystallogr.* **1994**, *B50*, 348−357.
(46) Steiner, T. *J. Chem. Soc., Chem. Commun.* **1995**, 1331−1332.
(47) Gilli, P.; Bertolasi, V.; Ferretti, V.; Gilli, G. *J. Am. Chem. Soc.* **1994**, *116*, 909−915.
(48) Steiner, T. *J. Phys. Chem. A* **1998**, *102*, 7041−7052.
(49) Steiner, T. *Angew. Chem., Int. Ed.* **2002**, *41*, 48−76.
(50) Grabowski, S. J. *J. Mol. Struct.* **2000**, *552*, 153−157.
(51) Pauling, L. *J. Am. Chem. Soc.* **1947**, *69*, 542−553.
(52) Brown, I. D. *Acta Crystallogr.* **1992**, *B48*, 553−572.

$\Delta ZPE(OH)°$ and $\Delta ZPE(HN)°$ represent the zero-point energy

$$\Delta ZPE = \Delta ZPE°(4p_{OH}p_{HN})^2 + \Delta ZPE(OH)°p_{OH} + \Delta ZPE(HN)°p_{HN} \quad (8)$$

differences of the hypothetical free diatomic states OH and HN as compared to the reference complex XHY. $\Delta ZPE°$ represents the absolute drop of zero-point energy between the non-hydrogen-bonded limiting states and the strongest hydrogen-bonded quasi-symmetric state. Equation 8 provides a link between the world of geometries, NMR parameters, and vibrations of hydrogen bonds. An example, the upper dotted line in Figure 4b, will be presented later.

The equations of this section refer to OHN-hydrogen-bonded systems where the proton does not exhibit a substantial barrier in the quasisymmetric case. To treat this case we use the following definitions,

$$\begin{array}{lcl} \text{tautomer } a & \text{A-H}\cdots\text{B + XDY} \overset{K_a}{\rightleftharpoons} & \text{A-D}\cdots\text{B + XHY} \\ & \Big\updownarrow K_t^H & \Big\updownarrow K_t^D \\ \text{tautomer } b & \text{A}\cdots\text{H-B + XDY} \overset{K_b}{\rightleftharpoons} & \text{A}\cdots\text{D-B + XHY} \end{array} \quad (9)$$

$K_a = 1/\phi_a$ and $K_b = 1/\phi_b$ represent the reciprocal fractionation factors of the two tautomeric states a and b with respect to the reference system. K_t^H and K_t^D represent the equilibrium constants of tautomerism of the protonated and the deuterated hydrogen bond, here the OHN-hydrogen bond of **1**. From eq 9 it follows that

$$K_a K_t^D = K_t^H K_b \quad (10)$$

and it follows that the fractionation factor of the tautomerism in AHB is given by

$$\phi_t = \frac{K_t^D}{K_t^H} = \frac{K_b}{K_a} \quad (11)$$

NMR Hydrogen Bond Correlations in the Absence and Presence of a Tautomeric Equilibrium. In several papers,[11−15] some of us have proposed correlating NMR parameters of hydrogen bonds not with distances but with the corresponding bond valences which reduce the number of adjustable parameters as the values of $r_i°$ and b_i are already known from the crystallographic data. The following relations were proposed for the chemical shifts and coupling constants of OHN-hydrogen bonds

$$\delta(\text{OL}\underline{\text{N}}) = \delta(\underline{\text{N}})°p_{\text{OL}}{}^{\text{L}} + \delta(\text{L}\underline{\text{N}})°p_{\text{LN}}{}^{\text{L}} + 4\delta(\text{OL}\underline{\text{N}})*p_{\text{OL}}{}^{\text{L}}p_{\text{LN}}{}^{\text{L}},\ \text{L} = \text{H, D} \quad (12)$$

$$\delta(\text{O}\underline{\text{HN}}) = \delta(\text{O}\underline{\text{H}})°p_{\text{OH}}{}^{\text{H}} + \delta(\underline{\text{H}}\text{N})°p_{\text{HN}}{}^{\text{H}} + 4\delta(\text{O}\underline{\text{HN}})*p_{\text{OH}}{}^{\text{H}}p_{\text{HN}}{}^{\text{H}} \quad (13)$$

$$^1J(\text{O}\underline{\text{HN}}) = {}^1J(\underline{\text{HN}})°p_{\text{HN}}{}^{\text{H}} - 8J(\text{O}\underline{\text{HN}})*(p_{\text{OH}}{}^{\text{H}})^2p_{\text{HN}}{}^{\text{H}} \quad (14)$$

We will use throughout this paper the isotopic sensitive bond valences in these equations in order to describe experimental data. The equilibrium bond valence can be used by the absence of isotope effects as a first approximation. $\delta(\underline{\text{N}})°$, $\delta(\text{L}\underline{\text{N}})°$, $\delta(\text{O}\underline{\text{H}})°$, and $\delta(\underline{\text{H}}\text{N})°$ represent the chemical shifts of the fictive free molecular units into which the OHN hydrogen bond can formally be dissociated, and $^1J(\underline{\text{HN}})°$, the one-bond coupling in the free fictive HN unit. $\delta(\text{OL}\underline{\text{N}})*$, $\delta(\text{O}\underline{\text{H}}\text{N})*$ and $J(\text{O}\underline{\text{H}}\text{N})*$ are "excess" terms which describe the deviation of the quasi-symmetric hydrogen bond from the average of the fictive limiting molecular units.

In the case of a fast equilibrium between two tautomeric forms a and b, any observed NMR chemical shift or coupling constant represents weighed averages over both forms characterized by the mole fractions x_a and x_b, e.g.,

$$\delta_{obsd} = x_a\delta_a + x_b\delta_b = \frac{\delta_a + K_t\delta_b}{1 + K_t} \quad (15)$$

which leads to expressions such as

$$K_t = \frac{x_b}{x_a} = \frac{\delta_{obsd} - \delta_a}{\delta_b - \delta_{obsd}} = \frac{J_{obsd} - J_a}{J_b - J_{obsd}} \quad (16)$$

We will identify form a with the enol-form and form b with the keto-form.

The theory of NMR parameters in the presence of equilibrium isotope effects is well established.[53−60] From eqs 11 and 15 it follows for any NMR chemical shift that

$$\delta_{obsd}^H = \frac{\delta_a^H + K_t^H\,\delta_b^H}{1 + K_t^H} \text{ and } \delta_{obsd}^D = \frac{\delta_a^D + K_t^D\,\delta_b^D}{1 + K_t^D} = \frac{\delta_a^D + \phi_t K_t^H\,\delta_b^D}{1 + \phi_t K_t^H} \quad (17)$$

We set

$$\delta_a^D = \delta_a^H - \Delta_a,\ \delta_b^D = \delta_b^H - \Delta_b \quad (18)$$

where Δ_a and Δ_b represent the intrinsic isotope effects on the chemical shifts in forms a and b. We obtain

$$\delta_{obsd}^D - \delta_{obsd}^H = \frac{\delta_a^H - \Delta_a + \phi_t K_t^H(\delta_b^H - \Delta_b)}{1 + \phi_t K_t^H} - \frac{\delta_a^H + K_t^H\,\delta_b^H}{1 + K_t^H} \quad (19)$$

For the case where $\phi_t = 1$ it follows that

$$\delta_{obsd}^D - \delta_{obsd}^H = -\frac{\Delta_a + K_t^H\Delta_b}{1 + K_t^H} \quad (20)$$

We call these isotope effects "equilibrium averaged intrinsic

(53) Siehl, H. U. *Adv. Phys. Org. Chem.* **1987**, *23*, 63−163.
(54) Bolvig, S.; Hansen, P. E. *Magn. Reson. Chem.* **1996**, *34*, 467−478.
(55) Perrin, C. L.; Nielson, J. B. *J. Am. Chem. Soc.* **1997**, *119*, 12734−12741.
(56) Perrin, C. L.; Kim, Y. J. *J. Am. Chem. Soc.* **1998**, *120*, 12641−12645.
(57) Perrin, C. L.; Thoburn, J. D. *J. Am. Chem. Soc.* **1989**, *111*, 8010−8012.
(58) Saunders, M.; Laidig, K. E.; Wolfsberg, M. *J. Am. Chem. Soc.* **1989**, *111*, 8989−8994.
(59) Saunders, M.; Telkowski, L.; Kates, M. R. *J. Am. Chem. Soc.* **1977**, *99*, 8070−8071.
(60) Saunders, M.; Kates, M. R. *J. Am. Chem. Soc.* **1977**, *99*, 8071−8072.

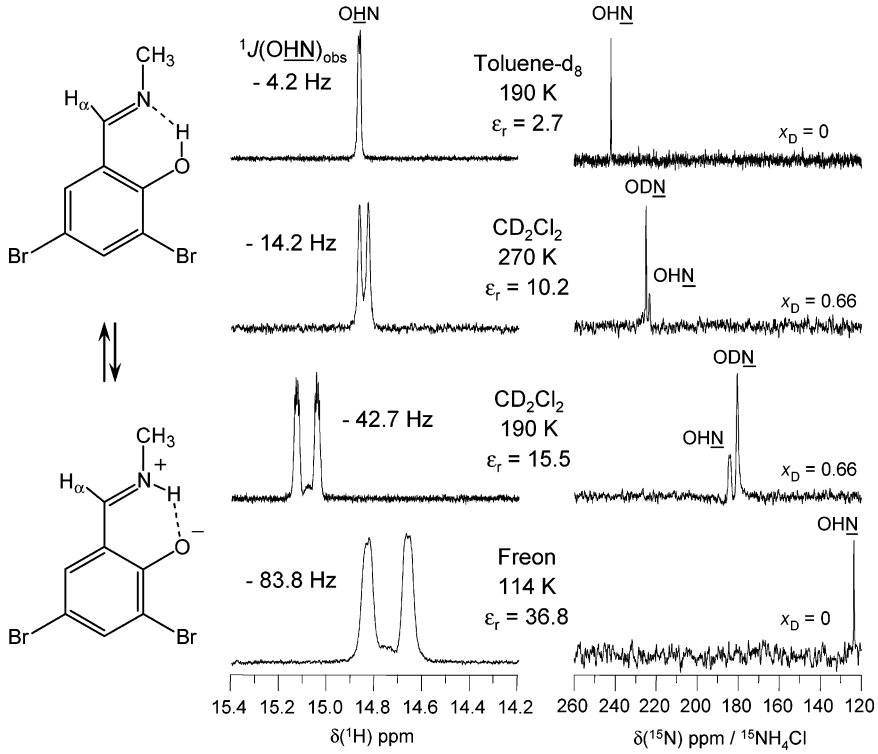

Figure 1. ^{1}H and ^{15}N{^{1}H} NMR spectra of **1** in a several aprotic solvents and temperatures. Toluene-d_8: 190 K; ^{1}H, 3mM; ^{15}N, 15mM. CD_2Cl_2: 270 and 190 K; ^{1}H, 2mM; ^{15}N, 45mM. $CDF_3/CDClF_2$ (0.4:0.6 Freon mixture): ^{1}H and ^{15}N, 3mM. The deuteration fractions x_D were estimated by integration of ^{1}H signals. NMR parameters and the static dielectric constants ϵ_r are listed in Table 1.

isotope effects", as isotopic fractionation is absent. In the symmetric case

$$\Delta_a = -\Delta_b = \Delta \text{ and } K_t^H = 1 \rightarrow \delta_{obsd}^D - \delta_{obsd}^H = 0 \quad (21)$$

i.e., the effect disappears.

The isotopic perturbation case described by Saunders[58−60] corresponds to the condition

$$\Delta_a = -\Delta_b = 0 \text{ and } K_t^H = 1 \quad (22)$$

for which it follows from eq 19 that

$$\frac{\delta_{obsd}^D - \delta_{obsd}^H}{\delta_a^H - \delta_b^H} = \frac{1 - \phi_t}{2(1 + \phi_t)} \quad (23)$$

Results

NMR Spectroscopy. An overview of the NMR signals of the OHN-hydrogen bond of **1** dissolved in various solvents at different temperatures, in the absence of alcohols, is presented in Figure 1, where the static dielectric constants ϵ_r were increased from the top to the bottom. The comparison of toluene and dichloromethane at 190 K shows that the NMR parameters strongly depend on ϵ_r which is smallest for toluene at 190 K and highest for the Freon mixture around 114 K. The signal of the hydrogen bond proton appears around δ(O$\underline{H}$N)$_{obs}$ = 15 ppm; at first sight, there is no special correlation with ϵ_r. However, the signals are split by scalar coupling with ^{15}N, where the coupling constant ^1J(O$\underline{H}$N)$_{obs}$ increases strongly with ϵ_r. At the same time, the ^{15}N signal characterized by δ(OH$\underline{N}$)$_{obs}$ is shifted from low to high field. H/D isotope effects are observed on these signals. At low values of ϵ_r, the one-bond isotope effect $^1\Delta\underline{N}(D) = \delta(OD\underline{N}) - \delta(OH\underline{N})$ is positive but becomes negative when ϵ_r is increased. An additional splitting of the OH signal, $^3J(\underline{H}_\alpha CN\underline{H})_{obs}$ arises from the coupling with the H-α proton, which represents a doublet (not shown), and also increases with ϵ_r. This signal is also slightly shifted when the hydrogen bond is deuterated. It is worth mentioning that in dichloromethane at 190 K the OH signal shows a more complex fine structure most probably due to the effect of the additional coupling with the methyl group protons.

Qualitatively, the above findings can be explained in terms of the tautomerism of Scheme 2, where the OH form dominates at low and the NH-form at high dielectric constants, as this form is zwitterionic and hence stabilized by a high solvent polarity.

In Figure 2 are depicted NMR spectra obtained of solutions of **1** in dichloromethane-d_2 at different molar ratios R of methanol with respect to **1**. The spectrum of **1** in pure methanol is also included. In addition, the signals H-4, H-6, and H-α and N−CH_3 are depicted, as well as the signals of AH = methanol. A$\underline{H}$ represents the hydroxyl proton (−O$\underline{H}$), and $\underline{A}$H, the methyl signal.

The addition of methanol leads to similar effects on the signals of the hydrogen bond nuclei of **1** as the increase of ϵ_r. $^1\Delta\underline{N}(D)$ is always negative but remains fairly constant. The low-field shift of H_α after deuteration is well pronounced, whereas the other signals of **1** exhibit little changes. The OH-signal of methanol shifts to low field as R is increased. It represents an average over monomeric methanol, self-associated methanol, and methanol hydrogen-bonded to **1**. Because of this complicated association scheme a quantitative analysis of the associated chemical shifts was not possible. We only note that the OH-signal absorbs at lower field in dichloromethane as compared to pure methanol, an effect which can be described to the

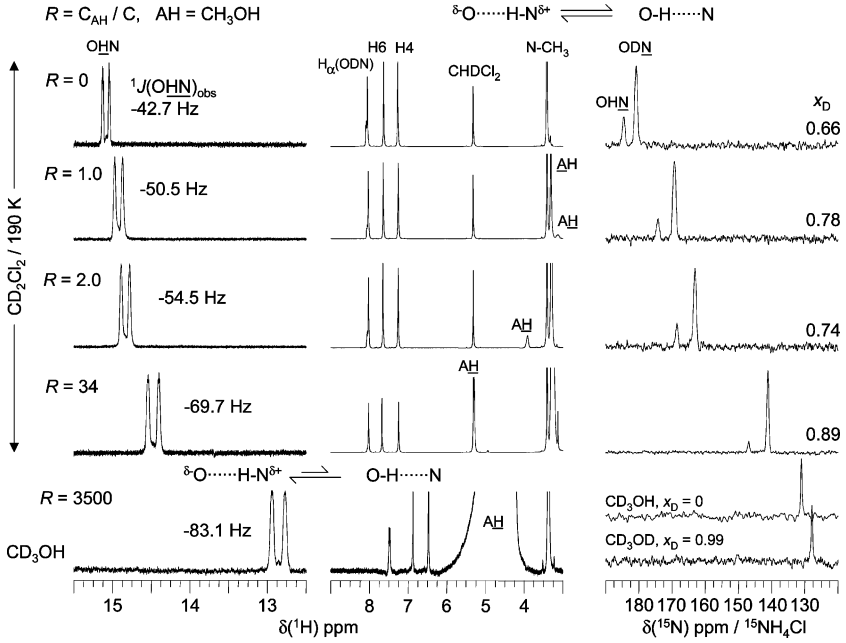

Figure 2. ^{1}H and ^{15}N{^{1}H}NMR spectra of **1** (45mM) in CD_2Cl_2 at 190 K in the presence of added methanol AH = CH_3OH/D. The ratio alcohol/substrate is defined as $R = C_{AH}/C$. *R* and the deuteration fractions x_D were estimated by integration of ^{1}H signals. NMR parameters are listed in Table 1.

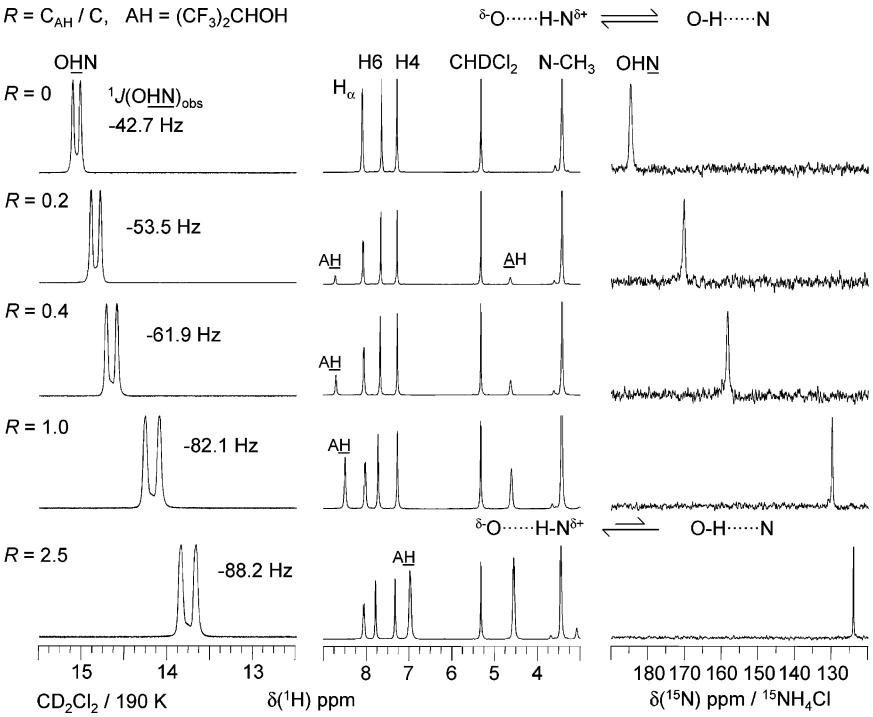

Figure 3. ^{1}H and ^{15}N{^{1}H} NMR spectra of **1** (30mM) in CD_2Cl_2 at 190 K, in the presence of added HFIP, AH = $(CF_3)_2CHOH$. The ratio alcohol/substrate is defined as $R = C_{AH}/C$. *R* values were estimated by integration of ^{1}H signals. NMR parameters are listed in Table 1.

circumstance that the hydrogen bond of methanol with 1 is stronger than with other methanol molecules.

The effects of the addition of HFIP, AH = $(CF_3)_2CHOH$, on the NMR signals of **1** are much more pronounced, as illustrated in Figure 3. Whereas the CH-signal, labeled as AH, is unaffected by the addition of alcohol, the OH signal, labeled as AH, appears around 8.8 ppm as long as *R* is smaller than unity. This means that already, at small concentrations of HFIP, a 1:1 complex with **1** is formed, in which the tautomeric equilibrium of **1** is substantially shifted to the NH-form. Only after adding a larger quantity of HFIP, a high-field shift is observed for its OH-signal, as the additional HFIP molecules can now only form self-associates whose hydrogen bonds are weaker than the one with **1**.

Finally, we have performed some preliminary experiments on *N*-(2-methoxybenzylidene)-methylamine **2** for comparison. A ^{15}N chemical shift of 279.5 ppm was obtained at natural abundance using {^{1}H} decoupling. By measuring the nondecoupled ^{15}N spectra of **1**−H$^+$ in trifluoroacetic acid solution, we obtained a one-bond coupling constant of $^1J(\underline{OHN})_{obs} = -93.86$ Hz and the ^{15}N chemical shifts $\delta(\underline{OHN})_{obs} = 149.68$ ppm and $\delta(\underline{ODN})_{obs} = 150.22$ ppm, i.e., $^1\Delta\underline{N}(D)_{obs} = -0.54$

Table 1. $^{1}H/^{15}N$ Chemical Shift, One-Bond $^{1}J(\underline{O}H\underline{N})$ and Three-Bond (Vicinal) $^{3}J(\underline{H}_{\alpha}C\underline{N}H)$ Coupling Constants and One-Bond Secondary Isotope Effect $^{1}\Delta N(D) = \delta(OD\underline{N}) - \delta(OH\underline{N})$ of **1** in a Variety of Solvents[o]

complex	solvent	T/K	ϵ_r	R	x_D	K_t	$\delta(OH\underline{N})$ /ppm	$^{1}J(OH\underline{N})$ /Hz	$^{3}J(\underline{H}_{\alpha}CNH)$[b]/ Hz	$\delta(OH\underline{N})$/ ppm	$\delta(OD\underline{N})$/ ppm	$^{1}\Delta N(D)$/ ppm	$\delta(A\underline{H})$/ ppm
2[a]	CD_2Cl_2	300	8.96[h]	0	0					279.50			
1	toluene-d_8	240	2.47[i]	0	0		14.48	−3.03		245.52			
	toluene-d_8	220	2.53[i]	0	0		14.62	−3.33		244.71			
	toluene-d_8	200	2.61[i]	0	0		14.78	−3.88		243.21			
	toluene-d_8	190	2.66[i]	0	0		14.86	−4.25		242.11			
	toluene-d_8	180	2.71[i]	0	0		14.95	−5.02		240.54			
1	$CDCl_3$	260	5.48[j]	0	0	0.22[m]	14.97	−19.11		218.2[e]	219.73[e]	1.53[e]	
	$CDCl_3$	250	5.72[j]	0	0	0.27[m]	15.04	−21.60		214.3[e]	215.36[e]	1.06[e]	
	$CDCl_3$	240	5.98[j]	0	0	0.33[m]	15.11	−24.52		208.7[e]	209.00[e]	0.30[e]	
	$CDCl_3$	230	6.26[j]	0	0	0.40[m]	15.17	−27.68		201.3[e]	200.69[e]	−0.61[e]	
	$CDCl_3$	205	7.07[j]	0	0	0.75[m]	15.28	−38.82	5.57	195.7[f]			
1	CD_2Cl_2	300	8.96[h]	0	0.66	0.13[m]	14.70	−14.21		229.43	231.64	2.22	
	CD_2Cl_2	270	10.22[h]	0	0.66	0.20[m]	14.85	−18.30		223.52	225.16	1.66	
	CD_2Cl_2	260	10.70[h]	0	0.66	0.23[m]	14.89	−19.94		220.90	222.29	1.39	
	CD_2Cl_2	250	11.23[h]	0	0.66	0.27[m]	14.94	−21.97		217.77	218.96	1.19	
	CD_2Cl_2	240	11.79[h]	0	0.66	0.33[m]	14.98	−24.46		214.08	214.94	0.86	
	CD_2Cl_2	230	12.41[h]	0	0.66	0.39[m]	15.02	−27.24		209.92	210.21	0.29	
	CD_2Cl_2	220	13.08[h]	0	0.66	0.47[m]	15.05	−30.12		205.13	204.58	−0.55	
	CD_2Cl_2	210	13.82[h]	0	0.66	0.58[m]	15.07	−33.83		199.26	197.52	−1.75	
	CD_2Cl_2	200	14.63[h]	0	0.66	0.71[m]	15.08	−37.85	5.65	192.24	189.72	−2.53	
	CD_2Cl_2	190	15.52[h]	0	0.66	0.92[m]	15.09	−42.74	6.32	183.94	180.63	−3.30	
1 + AH(HFIP) (= $(CF_3)_2CHOH$)	CD_2Cl_2	190		0.2	0		14.84	−53.57	8.08	170.31			8.72
	CD_2Cl_2	190		0.4	0		14.65	−61.91	9.16	158.42			8.70
	CD_2Cl_2	190		1.0	0		14.18	−82.07	12.18	129.94			8.49
	CD_2Cl_2	190		2.5[d]	0		13.76	−88.23	13.32	124.11			6.97[g]
1 + AH (= CH_3OH)	CD_2Cl_2	190		1.0	0.78		14.92	−50.56	6.68	174.29	169.32	−4.98	3.13
	CD_2Cl_2	190		1.6	0.82		14.87	−52.88	6.87	170.74	165.51	−5.23	3.62
	CD_2Cl_2	190		2.0	0.74		14.84	−54.54	7.59	168.56	163.10	−5.46	3.92
	CD_2Cl_2	190		22	0.92		14.52	−67.83	8.93	149.42	143.49	−5.93	5.23
	CD_2Cl_2	190		34	0.89		14.47	−69.68	9.43	146.91	141.10	−5.80	5.30
	CD_3OH	190	55.60[k]	3500	0		12.76	−83.09	12.79	131.07			4.80
	CD_3OD	190		3500	0.99						127.86	−3.21	
1	Freon	190	16.26[l]	0	0	1.15[n]	15.38	−48.75	7.10				
	Freon	180	17.88[l]	0	0	1.56[n]	15.35	−54.80	7.99				
	Freon	170	19.72[l]	0	0	2.24[n]	15.29	−61.30	8.94				
	Freon	160	21.81[l]	0	0	3.42[n]	15.21	−67.88	9.94				
	Freon	150	24.20[l]	0	0	5.44[n]	15.12	−73.57	10.74				
	Freon	140	26.98[l]	0	0	9.01[n]	15.01	−78.01	11.38	133.22			
	Freon	130	30.24[l]	0	0	18.7[n]	14.90	−81.93	11.91	127.79			
	Freon	120	34.12[l]	0	0	30.3[n]	14.80	−83.44	12.22	124.81			
	Freon	114	38.81[l]	0	0	35.7[n]	14.75	−83.82	12.25	123.63			
1 + AH (= CH_3OH)	Freon	130		0.9	0		14.73	−83.13	12.16	126.34			5.14
	Freon	130		1.8	0		14.66	−83.87	12.10	125.93			5.66
	Freon	130		63	0		14.41	−85.93	12.53	124.20			5.97
1−H^+	CF_3CO_2H	300		0	0			−93.86[c]		149.68			
	CF_3CO_2D	300		0	0.99						150.22	0.54	

[a] The dependence of the static dielectric constanats ϵ_r were calculated using the equation $\epsilon_r(T) = A + B/(T - C)$.[33,61,62] $^{15}N\{^{1}H\}$ NMR natural abundance spectra of neat liquid **2** recorded by locking on a dichloromethane-d_2 capillary. [b] Could not be measured for values below 4 Hz. [c] Coupling constant obtained from non-^{1}H-decoupled ^{15}N NMR spectra. [d] HFIP precipitates. [e] Obtained from ref 26. [f] Obtained from ref 28, $\delta(OH\underline{N})$ at 205.5 K. [g] $\delta(A\underline{H}) = 4.5$ ppm of free HFIP at 190 K in CD_2Cl_2. [h] CH_2Cl_2[63]: $A = -2.3749$, $B = 3401$ K, and $C = 0$. [i] Toluene-h_8[64,65]: $A = 1.749\,52$, $B = 172$ K, and $C = 0$. [j] $CHCl_3$[63] using $A = -0.4924$, $B = 1554$ K, and $C = 0$. [k] Methanol,[66,67]: $A = -10.1369$, $B = 12\,491$ K, and $C = 0$. [l] Freon mixture with a CDF_3 mole fraction of 0.4, ϵ_r were calculated by using the empirical relation from ref 33. [m] Calculated by using eq 24 and the limiting values of situation 2 listed in Table 3. [n] Similar, but limiting values of situation 3. [o] Ratio alcohol to **1**: $R = C_{AH}/C$, where AH = CH_3OH/D or $(CF_3)_2CHOH$. R and deuteration fraction x_D were estimated by integration of ^{1}H signals. In CD_2Cl_2 comparisons with the nondeuterated **1** identify the $\delta(OD\underline{N})$ chemical shift. By addition of methanol the highest peak was assigned to be $\delta(OD\underline{N})$. ^{15}N chemical shifts are referenced to external solid $^{15}NH_4Cl$.

ppm. We tentatively assign the structure included in Scheme 2 to this species. Unfortunately, we could neither observe the proton in the OHO-hydrogen bond nor establish whether two or only one H-bond is formed between the two species.

The results of all NMR measurements are assembled in Table 1.

DFT Calculations. To correlate the NMR parameters with hydrogen bond geometries we have performed DFT calculations of the intramolecular OHN-hydrogen-bond geometries, in particular the distances r_{NH}, r_{OH}, and r_{NO}, of the series of *N*-(R_1-salicylidene)-alkyl(R_2)amine derivatives depicted in Scheme 4 and Table 2. In addition, GIAO calculations of the ^{15}N chemical shifts were carried out (see Supporting Information). By comparison of the calculated heavy atom distances r_{NO} of the **B**, **D**, and **H** with the crystallographic r_{NO} distances,[61−69] we have estimated a margin of error of 5%. This was confirmed by additional MP2 calculations of **B**, **D**, and **H** which are appropriate to calculate hydrogen bond geometries. For each

Table 2. Calculated Geometries of the Intramolecular OHN-Hydrogen Bond of the Tautomer a (OH-Form) and b (NH-Form) of *N*-(R_1-Salicylidene)-alkyl(R_2)amines {Method: DFT (B3LYP/6-31++G(d))}

Tautomer b (NH-Form)

	N-(R_1-salicylidene)-alkyl(R_2)amines	R_1	R_2	r_{NO}/Å	r_{OH}/Å	r_{NH}/Å	α(OHN)/deg
A	*N*-(5-methoxy-	5-OCH_3	$-CH_3$	2.604	1.741	1.038	137.61
B	*N*-(5-chloro-	5-Cl	$-CH_3$	2.603	1.734	1.040	138.10
C	*N*-(3-methoxy-	3-OCH_3	$-CH_3$	2.602	1.741	1.038	137.32
D	*N*-(3,5-dichloro-	3,5-diCl	$-CH_3$	2.602	1.741	1.039	137.35
E	*N*-(3,5-dibromo-	3,5-diBr	$-CH_3$	2.596	1.731	1.040	137.68
F	*N*-(4-methoxy-	4-OCH_3	$-CH_3$	2.599	1.722	1.043	138.75
G	*N*-(4,6-dimethoxy-	4,6-diOCH_3	$-CH_3$	2.592	1.722	1.041	138.13
H	*N*-(5-nitro-	5-NO_2	$-C_2H_5$	2.607	1.743	1.039	137.71
I	*N*-(3,4,5,6-tetrafluoro-	3,4,5,6-tetraF	$-CH_3$	2.618	1.764	1.036	136.93

Tautomer a (OH-Form)

	N-(R_1-salicylidene)-alkyl(R_2)amines	R_1	R_2	r_{NO}/Å	r_{OH}/Å	r_{NH}/Å	α(OHN)/deg
A	*N*-(5-methoxy-	5-OCH_3	$-CH_3$	2.660	0.996	1.773	146.21
B	*N*-(5-chloro-	5-Cl	$-CH_3$	2.653	0.998	1.763	146.43
C	*N*-(3-methoxy-	3-OCH_3	$-CH_3$	2.651	0.998	1.759	146.89
D	*N*-(3,5-dichloro-	3,5-diCl	$-CH_3$	2.636	1.001	1.739	147.03
E	*N*-(3,5-dibromo-	3,5-diBr	$-CH_3$	2.635	1.001	1.738	147.03
F	*N*-(4-methoxy-	4-OCH_3	$-CH_3$	2.656	0.999	1.761	147.07
G	*N*-(4,6-dimethoxy-	4,6-diOCH_3	$-CH_3$	2.619	1.004	1.714	147.87
H	*N*-(5-nitro-	5-NO_2	$-C_2H_5$	2.667	0.995	1.782	146.25
I	*N*-(3,4,5,6-tetrafluoro-	3,4,5,6-tetraF	$-CH_3$	2.626	1.004	1.727	146.92

Scheme 4. Overview of a Series of Schiff Bases, *N*-(R_1-Salicylidene)-alkyl(R_2)amines, Calculated Using the Density Function Method (B3LYP/6-31++G(d))

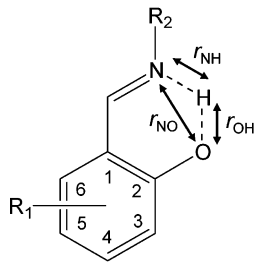

A: R_1 = 5-OCH_3, R_2 = CH_3
B: R_1 = 5-Cl, R_2 = CH_3
C: R_1 = 3-OCH_3, R_2 = CH_3
D: R_1 = 3,5-diCl, R_2 = CH_3
E: R_1 = 3,5-diBr, R_2 = CH_3
F: R_1 = 4-OCH_3, R_2 = CH_3
G: R_1 = 3,5-diOCH_3, R_2 = CH_3
H: R_1 = 5-NO_2, R_2 = C_2H_5
I: R_1 = 3,4,5,6-tetraF, R_2 = CH_3

structure in **A** to **I** series, the geometries of the two forms, namely, NH- and OH-tautomers, were calculated and the geometries of the both forms are reported in Table 2.

Discussion

We have studied the NMR parameters of **1** in the presence of the tautomeric equilibrium of Scheme 2. An increase of the dielectric constant shifts the equilibrium from tautomer a toward tautomer b. This observation is consistent with the zwitterionic NH form depicted in Scheme 2. One does not expect such a behavior for a neutral quinoid form which exhibits a much smaller dipole moment. Added HFIP forms at low concentration a 1:1 complex with **1**, which further favors the zwitterionic NH form as illustrated in Scheme 2. The proton-donating power of methanol is smaller; its effects are somewhere between a specific and a global solvation of **1**. Finally, H/D isotope effects on the ^{15}N chemical shifts of **1** have been observed.

The problem arises to separate the observed effects into intrinsic effects, associated with geometric changes of each tautomer as a function of the environment and into effects of the tautomeric equilibrium, which is a function of the environment as well. For this purpose, in this section, we will analyze the NMR data assembled in Table 1 using the NMR hydrogen bond correlations described in the theoretical section.

The results of our data analysis are depicted in Figures 4−6. The parameters used in order to calculate the theoretical curves are assembled in Table 3. First, we will describe each graph separately and justify the choice of the parameter sets later.

Geometric OHN Hydrogen Bond Correlation. The dashed line in Figure 4a represents the correlation between the hydrogen bond coordinates q_2 and q_1 which refer to the equilibrium geometries where zero-point vibrations are not taken into account. According to eqs 1 and 2, the correlation line depends only on the values of $r_1°$ and $r_2°$, the equilibrium distances in the fictive free diatomic units AH and HB, and of b_1 and b_2, the decay parameters of the bonds when they are stretched. We note that the equilibrium geometries of the tautomers a and b of compounds **A** to **I** (Scheme 4) calculated using the density function method are well located on the dashed equilibrium correlation curve. In the dotted line of Figure 4a an empirical correction for zero-point motions is included by using nonzero parameters c^H and d^H in eq 3, derived previously[17] for the OHN-hydrogen bond of pyridine with proton donors of the type ROH. However, the approximation that a given hydrogen bond can be described sufficiently well in terms of single average geometries is still maintained. In the remaining graphs, we omit the equilibrium correlation curves.

Along this line, we describe then a two-state tautomeric equilibrium in terms of a combination of two geometries corresponding to tautomers a as well as b as illustrated for at first sight four arbitrary situations in Figure 4a. Situation 1 corresponds to an equilibrium between a tautomer a containing a weaker O−H···N hydrogen bond and tautomer b containing a stronger $^-$O···H−N$^+$ hydrogen bond. By contrast, situation 4 corresponds to an equilibrium between a tautomer a containing a stronger O−H···N hydrogen bond and tautomer b containing

(61) Grant, R. F.; Davidson, D. W.; Gray, P. *J. Chem. Phys.* **1960**, *33*, 1713−1718.
(62) Carvajal, C.; Tolle, K. J.; Smid, J.; Szwarc, M. *J. Am. Chem. Soc.* **1965**, *87*, 5548−5553.
(63) Morgan, S. O.; Lowry, H. H. *J. Phys. Chem.* **1930**, *34*, 2385−2432.
(64) Matsuike, Y. *Proc. Imp. Acad. (Tokyo)* **1929**, *5*, 29−31.
(65) Richards, T. W.; Shipley, J. W. *J. Am. Chem. Soc.* **1919**, *41*, 2002−2012.
(66) Isnardi, H. *Z. Phys.* **1922**, *9*, 153−179.
(67) Le Fevre, R. J. W. *Trans. Faraday Soc.* **1938**, *34*, 1127−1132.
(68) Filarowski, A.; Koll, A.; Glowiak, T.; Majewski, E.; Dziembowska, T. *Ber. Bunsen-Ges. Phys. Chem.* **1998**, *102*, 393−402.
(69) Krygowski, T. M.; Wozniak, K.; Anulewicz, R.; Pawlak, D.; Kolodziejski, W.; Grech, E.; Szady, A. *J. Phys. Chem. A* **1997**, *101*, 9399−9404.

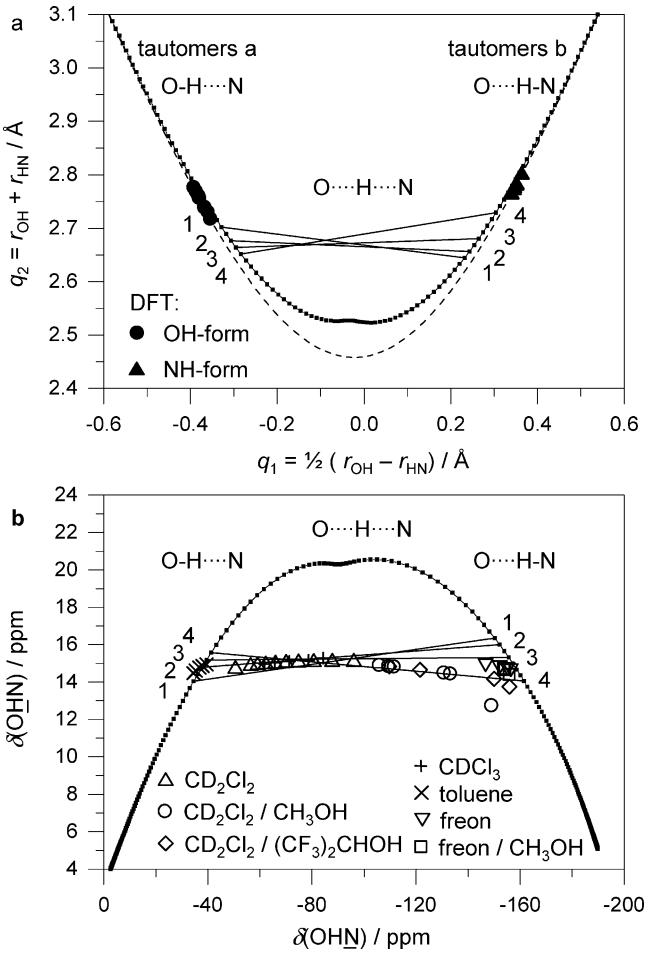

Figure 4. (a) Geometric OHN-hydrogen bond correlation of **1**, i.e., $q_2 = r_{OH} + r_{HN}$ as a function of $q_1 = {}^1/_2(r_{OH} - r_{HN})$. Equilibrium correlation, where zero-point vibrations are not taken into account, curve (dashed) and corrected correlation curve (dotted) calculated according to ref 17. Filled symbols: equilibrium geometries (Table 2) of several Schiff bases **A** to **I** (Scheme 4) calculated using DFT methods [B3LYP/6-31++G(d)]. "Tautomer" lines 1 to 4 are included which represent the average geometries in the presence of a tautomeric equilibria between tautomers of type a (OH-form, left side) and tautomers of type b (NH-form, right side), where the equilibrium constants K increase from the left to the right. When the dielectric constants are increased, the tautomer equilibrium 1 is continuously shifted to tautomeric equilibrium 4. (b) ^{1}H vs ^{15}N chemical shift correlation of Schiff base **1** under various conditions. For the calculation of the correlation curves, see text.

a weaker $^-$O···H−N$^+$ hydrogen bond. The dipole moments of both states increase from situation 1 to 4, also the hydrogen bond strength of tautomer a, but the hydrogen bond strength of tautomer b is weakened. Situation 1 is more typical for low dielectric constants, and situation 4, for large dielectric constants. As the latter increases with decreasing temperature, for a given solvent, the whole equilibrium is shifted on the correlation curve from situation 1 to situation 4. Note, the data points represented by the solid "tautomer" lines 1 to 4, linking the corresponding tautomers a and b, can be interpreted in terms of hydrogen bond geometries averaged by the tautomeric equilibrium.

OHN Geometry−NMR Parameter Correlation. As shown before,[17] the geometric hydrogen bond correlation of Figure 4a is the source of a similar NMR correlation between the ^{1}H and the ^{15}N chemical shifts depicted by the dotted line in Figure 4b. The latter are an excellent measure of the proton position, and the former, of the hydrogen bond compression. The

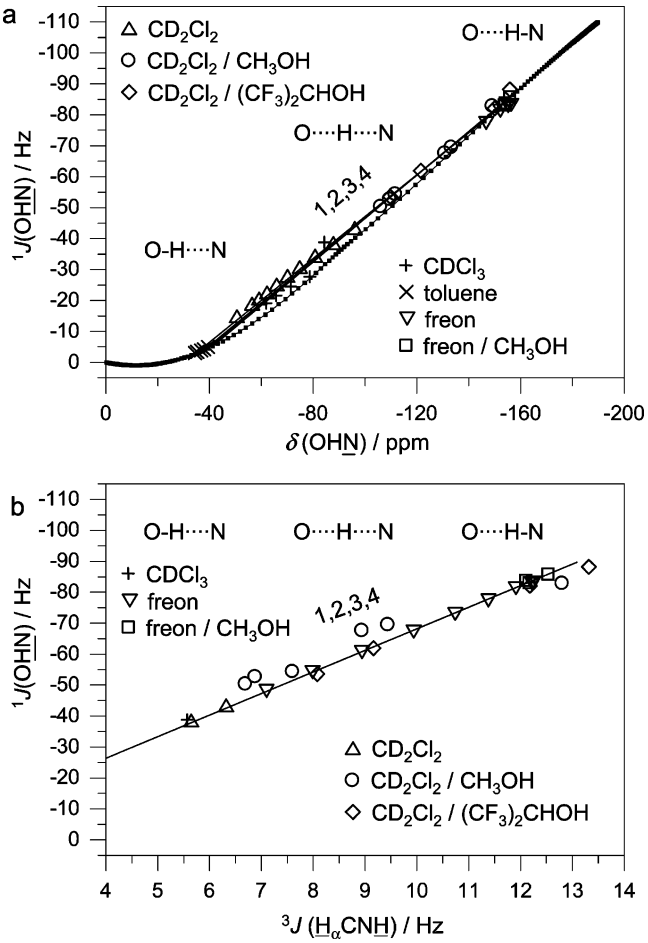

Figure 5. (a) ^{1}H−^{15}N scalar couplings vs ^{15}N chemical shift correlation of Schiff base **1** under various conditions. (b) ^{1}H−^{15}N scalar couplings, one-bond ^1J(OHN) vs three-bond (vicinal) ^3J(H_αCNH), besides the empirical linear relationship of ^1J(OHN) = −6.977^3J(H_αCNH) + 1.55 Hz can be mentioned. For further explanation, see text.

experimental data points of **1** are not at all located on the correlation curve, in contrast to the case of intermolecular pyridine−acid complexes.[17] These deviations are then the first indication of a tautomeric equilibrium.

The tautomer lines of Figure 4a are transformed now to those depicted in Figure 4b. They represent well the experimental data points of **1**. When the equilibrium constant K_t is increased, a data point is shifted along a given tautomer line from the left to the right. The experimental data indicated that a single tautomer line is not sufficient to describe the whole body of data. The graph indicates that $K_t \approx 0$ in the case of toluene as solvent, i.e., that the observed chemical shift changes are intrinsic and not affected by the tautomerism. Roughly, line 2 describes well the situation in dichloromethane and chloroform, whereas line 4 represents well the situation in the Freon mixture and in the presence of alcohols.

In addition to the ^{1}H chemical shifts, also the one-bond coupling constants ^1J(OHN) of **1** correlate with the ^{15}N chemical shifts as illustrated in Figure 5a. The dotted line corresponds to the intrinsic geometries and was calculated according to eq 14. The tautomer lines were calculated in a similar way as in Figure 4b. However, in contrast to the latter, they are not well-resolved in Figure 5a. We note that the coupling constants in the quasi-symmetric configuration are only slightly larger for the case of equilibrium as compared to the single-well situation where the

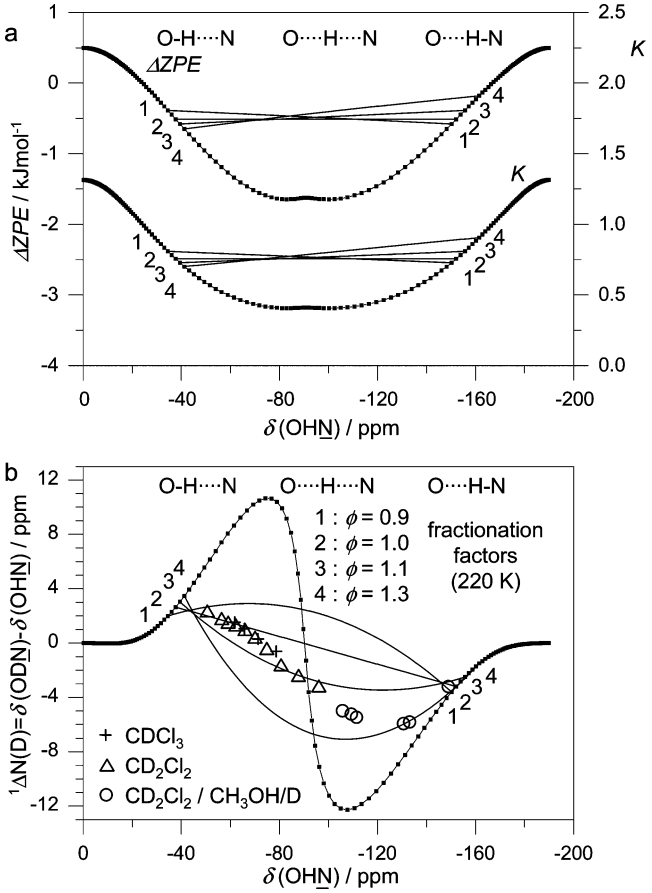

Figure 6. (a) Isotopic fractionation constant K (lower curve) and zero-point energy differences ΔZPE (upper curve) as a function of the ^{15}N chemical shifts of OHN-hydrogen bonds according to refs 14 and 17. (b) One-bond secondary D/H isotope effects vs ^{15}N chemical shifts. The dotted line represents the intrinsic isotope effects. The solid lines represent the tautomerism averaged values which depend both on the intrinsic and on the equilibrium isotope effects characterized by the fractionation factors ϕ_t at the average temperature 220 K of tautomerism between tautomers a and b. For further explanation, see text.

Table 3. Parameters of the NMR Hydrogen Bond Correlations of **1**[a,b]

Intrinsic NMR Parameters

δ(N)° /ppm	δ(HN)° /ppm	δ(OHN)* /ppm	δ(OH)° /ppm	δ(HN)° /ppm	δ(OHN)* /ppm	^1J(HN)° /Hz	J(OHN)* /Hz
0[b]	−190[c]	−5	3	5	20	−110	18

Intrinsic and Equilibrium Averaged Parameters

	δ(OHN)$_a$ enol /ppm	δ(OHN)$_b$ keto /ppm	Δ$_a$ enol /ppm	Δ$_b$ keto /ppm	δ(OHN)$_a$ enol /ppm	δ(OHN)$_b$ keto /ppm	^1J(OHN)$_a$ enol /Hz	^1J(OHN)$_b$ keto /Hz	ϕ_t[d]
1	−35	−150	2.0	−3.6	14.0	16.3	−3	−82	0.90
2	−37	−152	2.6	−3.2	14.8	16.0	−5	−84	1.00
3	−39	−155	3.0	−2.5	15.2	15.3	−6	−86	1.11
4	−41	−161	3.5	−1.5	15.6	14.0	−7	−90	1.29

[a] The geometric OHN-correlation parameters in eq 3 are $c^H = 360$, $d^H = 0.7$, $c^D = 30$, $d^D = 0.6$, and $f = 5$, $g = 2$. [b] ^{15}N chemical shifts in Figures 4 to 6 are with respect to neat liquid **2**, at 280 ppm. [c] Predicted using the empirical linear relationship, ^1J(OHN) = 0.69 [Hz/ppm] δ(OHN) +21.15 Hz, using the limiting coupling constants ^1J(HN)°. [d] The fractionation factors ϕ_t are calculated for the average temperature 220 K.

proton is located in the hydrogen-bond center. Therefore, the coupling constants are not of a diagnostic value in order to distinguish double- and single-well situations. However, if an equilibrium situation has been proved, for example, by a plot such as Figure 4b, then the coupling constants provide information about the equilibrium constant, as long as the corresponding intrinsic values can be obtained from a plot such as Figure 5a. For this purpose, we rewrite eq 16 in the form

$$K_t = \frac{x_b}{x_a} = \frac{^1J(\underline{OHN})_{obsd} - {}^1J(\underline{OHN})_a}{J(\underline{OHN})_b - {}^1J(\underline{OHN})_{obsd}} \qquad (24)$$

Here, $^1J(\underline{OHN})_a$ and $^1J(\underline{OHN})_b$ represent the intrinsic values given by eq 14, corresponding to the intersections of the tautomer lines 1 to 4 with the intrinsic dotted curve in Figure 5a. In approximation, one may use average intrinsic values characterizing a given solvent and temperature range. A similar equation can be written for the vicinal coupling. It is then easy to show that both couplings depend linearly on each other

$$^1J_{obsd} = {}^3J_{obsd}\frac{(^1J_b - {}^1J_a)}{(^3J_b - {}^3J_a)} - \frac{^1J_b{}^3J_a + {}^1J_a{}^3J_b}{(^3J_b - {}^3J_a)}$$

with $$^1J \equiv {}^1J(\underline{OHN}) \text{ and } {}^3J \equiv {}^3J(\underline{H}_\alpha CN\underline{H}) \qquad (25)$$

This equation was very well fulfilled; see Figure 5b. A problem for the calculation of K_t from observed values is that the intrinsic coupling constants in these equations depend on the solvent, dielectric constant, temperature; i.e., on which tautomer line 1 to 4, a given observed value is located.

Intrinsic vs Equilibrium H/D Isotope Effects on the ^{15}N Chemical Shifts of 1. In Figure 6a we have plotted the zero-point energy difference (ΔZPE) of a typical OHN-hydrogen bond as a function of the ^{15}N chemical shifts. The dotted line was calculated according to eq 8, and the parameters are taken from refs 14 and 17. The reference state XHY with ΔZPE = 0 corresponds to the complex of pyridine with triphenylmethanol.[14] We also plot the corresponding equilibrium constants K of the isotopic exchange with the reference state (eq 5), at an average temperature of 220 K. In the fictive limiting diatomic units OH or NH, ΔZPE is largest as no hydrogen bond is formed, i.e., as the stretching vibrations exhibit high frequencies. When a strong hydrogen bond is formed, ΔZPE is considerably reduced.

According to eq 11, the isotopic fractionation factor $\phi_t = K_t^D/K_t^H$ of the tautomerism is given by the ratio of the equilibrium constants K_b/K_a of the isotopic exchange reactions of each tautomer with the reference state as defined in eq 9. This allows us to associate a given value of ϕ_t for each of the tautomer lines, and we could calculate the tautomerism averaged H/D isotope effects on the nitrogen chemical shifts of **1**. These values are plotted in Figure 6b as a function of the ^{15}N chemical shifts.

Again, the dotted line corresponds to the intrinsic isotope effects calculated using eq 12 for a temperature of 220 K. We checked that changing the temperature in this equation leads only to minor changes of the resulting calculated curves.

Tautomer lines 1 to 4 were constructed using eq 19. As in situation 1, the hydrogen bond strength increases and ΔZPE decreases as tautomer b is formed, ϕ_t is smaller than 1, and the corresponding tautomer line for situation 1 exhibits an upward curvature. In the case of situation 2, ϕ_t was close to 1, and a straight line results, corresponding to the case of "equilibrium averaged intrinsic isotope effects". For situations 3 and 4, we obtain downward curved lines.

The comparison with the experimental data is quite satisfactory. Again line 2 describes well the situation in dichloromethane and chloroform, whereas line 4 seems to represent well the addition of methanol. Thus, decreasing temperature or increasing the dielectric constant, as well as specific solvation by an additional hydrogen bond according to Scheme 2, strengthens the hydrogen bond in the OH-form and reduces its zero-point energy, whereas the contrary is true for the NH-form.

Determination of the Correlation Parameters. The parameters obtained from the data analyses are assembled in Table 3. As a starting point, we used the parameters of the geometric OHN-correlation and of the Figure 4a (dotted line) as described above, taken from ref 17, derived for a large body of OHN-hydrogen bonded systems, by using Steiner's[48] proposed parameter set for OHN-hydrogen bonds $r_{OH}° = 0.942$ Å, $r_{HN}° = 0.992$ Å, $b_{OH} = 0.371$ Å, $b_{HN} = 0.385$ Å. The parameters of the ΔZPE correlation of eq 8 were taken from refs 14 and 17, derived for pyridine−acid complexes. The limiting chemical shifts and coupling constants needed to construct the correlation curves of Figures 4 to 6 were then adapted in the next step. All parameters depend on each other, and it was very tedious to obtain the data fit of Figures 4 to 6. In view of all assumptions made, we do not claim that the parameter set obtained is unique, but it was the only consistent parameter set which we could find within the limits of the valence bond order model. The graphs of Figures 4 to 6 show nicely the intrinsic and the equilibrium contributions to the NMR parameters, especially to the H/D isotope effects on the ^{15}N chemical shifts.

Thermodynamics of Tautomerism of 1. For the tautomeric equilibrium in many Schiff bases, $\Delta H°$ and $\Delta S°$ have been defined by UV−vis[21] spectroscopy and ^{13}C[22,70,71] NMR. For aniline Schiff bases of naphthylidene and salicylidene,[72,73] thermodynamic values have been obtained mainly from the temperature dependences of one-bond $^1H-^{15}N$ coupling or from the three-bond vicinal coupling constants. By inspection of Figure 4b, we noticed that line 2 describes well the situation in dichloromethane and chloroform, whereas line 3 seems to represent well the situation in the Freon mixture. The limiting values of the coupling constants $^1J(O\underline{H}N)_a$ and $^1J(O\underline{H}N)_b$ in the enol-form a and the keto-form b corresponding to these situations are listed in Table 3. These values were inserted into eq 24 in order to calculate the equilibrium constants K_t of the tautomerism of **1** listed in Table 1.

We note that $^1J(O\underline{H}N)_a$ corresponds to a weak coupling across the hydrogen bond and has, therefore, often been neglected in eq 24. Only in one case a coupling of 1.55 Hz was reported by Kurkovskaya,[74] but the sign of it is still unclear. It was shown by Pietrzak et al.[75] that in intramolecular NHN-hydrogen-bonded systems the sign of such a small coupling can be positive. We note again that the sign of the coupling obtained from Kurkovskaya[74] can be positive or negative. On the other hand, in our correlation analysis we provide evidence for substantial values of the order of −5 to −6 Hz. Values of $^1J(O\underline{H}N)_b$ of tautomer b have been estimated to be in the range between −89 and −96 Hz.[27,72,73,76−78] Here, we found smaller values of −84 to −86 Hz for situations 2 and 3. These intrinsic values are better justified than those previously, and hence the equilibrium constants calculated exhibit smaller systematic errors than those reported before. Thus, also the use of the coupling constants measured for Schiff bases dissolved in trifluoroacetic acid as a limiting value for $^1J(O\underline{H}N)_b$ will lead to erroneous equilibrium constants. For this solvent a room-temperature value of −92.5 Hz was reported by Kurkowskaya et al.[72] for an aniline Schiff base. For **1** we find under similar conditions a similar value of −93.9 Hz and a ^{15}N chemical shift of 149 ppm (Table 1). These values are quite different for tautomer b in Freon at low temperatures, exhibiting a $^1H-^{15}N$ coupling constant of −84 Hz and a ^{15}N chemical shift of 124 ppm. This difference may perhaps be explained in the future in terms of a double hydrogen bond structure as illustrated in Scheme 2.

Table 4. Thermodynamic Parameters of the Tautomeric Equilibrium of **1**

solvents	$\Delta H_t°$ kJ/mol	$\Delta S_t°$ J/K mol
CD_2Cl_2	−8.32 ± 0.13	−43.83 ± 0.55
Freon mixture	−8.56 ± 0.32	−43.41 ± 2.19
$CDCl_3$	−9.90 ± 0.14	−50.61 ± 0.59

Finally, we have plotted the ln K vs $1/T$ and found linear van't Hoff relations in the temperature range covered from which the enthalpies $\Delta H_t°$ and entropies $\Delta S_t°$ of the tautomerism in Scheme 2 in the absence of alcohol could be obtained. The parameters are listed in Table 4. $\Delta H_t°$ and $\Delta S_t°$ do not vary much for the different aprotic solvents. The major effect on the equilibrium is the change of the static dielectric constant ϵ_r.

Conclusions

We have studied the NMR properties of *N*-(3,5-dibromosalicylidene)-methylamine **1** dissolved in polar organic solvents, in the absence and the presence of added alcohols and have performed DFT calculations which assist the interpretation of the data obtained. **1** can serve as a model for the intramolecular hydrogen bond of Pyridoxalphosphate (PLP, Vitamine B6). This coenzyme is normally linked as an internal aldimine in the active site of the enzyme. These systems exhibit a keto−enol tautomeric equilibrium between an OH and a zwitterionic NH form. It was demonstrated that the increase of the dielectric constant of the aprotic solvent shifts the equilibrium toward the NH form. To model the PLP−water interaction in the active site of the enzyme, different alcohols were added to **1** dissolved in aprotic solvents. It was shown that this addition further stabilizes the NH form. The size of the effect is also dependent on the acidity of the added alcohol.

There are two types of conclusions which arise from this work. The first one is a methodological one. An important first step has been made toward a distinction of intrinsic and equilibrium H/D isotope effects of OHN-hydrogen-bonded systems. For this purpose the valence bond order model derived previously for intermolecular strong hydrogen bonds was further

(70) Salman, S. R.; Farrant, R. D.; Lindon, J. C. *Spectrosc. Lett.* **1991**, *24*, 1071−1078.
(71) Alarcon, S. H.; Olivieri, A. C.; Gonzalez-Sierra, M. *J. Chem. Soc., Perkin Trans. 2* **1994**, 1067−1070.
(72) Kurkovskaya, L. N.; Nurmukhametov, R. N.; Shigorin, D. N. *Zh. Strukt. Khim.* **1980**, *21*, 61−70.
(73) Dudek, G. O.; Dudek, E. P. *J. Am. Chem. Soc.* **1964**, *86*, 4283−4287.
(74) Kurkovskaya, L. N. *Zh. Strukt. Khim.* **1978**, *19*, 946−949.
(75) Pietrzak, M.; Limbach, H. H.; Perez-Torralba, M.; Sanz, D.; Claramunt, R. M.; Elguero, J. *Magn. Reson. Chem.* **2001**, *39*, 100−108.
(76) Dudek, G. O.; Dudek, E. P. *J. Am. Chem. Soc.* **1966**, *88*, 2407−2412.
(77) Salman, S. R.; Lindon, J. C.; Farrant, R. D.; Carpenter, T. A. *Magn. Reson. Chem.* **1993**, *31*, 991−994.
(78) Lycka, A.; Snobi, D. *Collect. Czech. Chem. Commun.* **1981**, *46*, 892−897.

developed. The results may be useful for future theoretical model studies of hydrogen bonds.

The second type of conclusion concerns the nature of the intramolecular OHN-hydrogen bond of **1** and, therefore, also of pyridoxal phosphate cofactor in aminotransferases. This bond is extremely sensitive to the local polarity and local hydrogen bonds to the oxygen. A high polarity favors the zwitterionic NH-forms which are only the reactive states in the enzymes. Thus, one can understand why the tyrosine and asparagine residues are needed (Scheme 1) in order to activate the enzyme.

Acknowledgment. This work was supported by the Deutsche Forschungsgemeinschaft, Bonn, and the Fonds der Chemischen Industrie, Frankfurt. We also thank the Russian Foundation of Fundamental Research, Moscow.

Supporting Information Available: NMR spectra of **1** and **2** in different aprotic and protic organic solvents are presented. Also information concerning the temperature dependence of the static dielectric constant ϵ_r and the full results of the DFT calculations of *N*-(R_1-salicylidene)-alkyl-(R_2)amines at DFT level of theory are included. Complete ref 37. This material is available free of charge via the Internet at http://pubs.acs.org.

JA056251V